

# Directionality in van der Waals Interactions: the Case of 4-Acetylbiphenyl Adsorbed on Au(111)

Vladimír Zobač,<sup>\*,†</sup> Roberto Robles,<sup>†</sup> and Nicolás Lorente<sup>†,‡</sup>

<sup>†</sup>*Centro de Física de Materiales CFM/MPC (CSIC-UPV/EHU)*

*Paseo Manuel de Lardizabal 5, E-20018 Donostia - San Sebastián, Spain.*

<sup>‡</sup>*Donostia International Physics Center (DIPC)*

*Paseo Manuel de Lardizabal 4, E-20018 Donostia - San Sebastián, Spain.*

E-mail: vladimir\_zobac001@ehu.eus

## Abstract

We report on a theoretical study of adsorption of 4-Acetylbiphenyl molecule and its diffusion properties in the main directions of the Au(111) surface. Structural changes of the molecule, which are induced by adsorption lead to stronger conjugation of the  $\pi$ -system. The molecule is adsorbed in a flat configuration on the surface with roughly the same binding energy along the  $[1\bar{1}0]$  and  $[11\bar{2}]$  directions, in good agreement with experiments. Furthermore, the diffusion barriers imply an important directionality of the molecule-surface interactions. This is somewhat surprising because our calculations show that the prevailing interaction is the long-range molecule-surface van der Waals interaction. Despite of its weakness, the van der Waals interaction discriminates the preferential adsorption sites as well as imposes a molecular geometry that needs to be considered when rationalizing the diffusion barriers.

# Introduction

New materials based on metal-organic interfaces offer promising properties in many applications concerning photovoltaic devices, sensors or heterogeneous catalysis.<sup>1-4</sup> The overlayer properties can be tuned by the nature of adsorbates and surface, as well as the way they assemble.

An important strategy to understand the interactions at play in the creation of molecular overlayers is atomic manipulation with scanning probes. The way molecules displace, assemble or dissociate under the action of such probes gives direct information of the forces joining them together and the role of the environment in the formation of collective structures. The various manipulation strategies include pushing molecules by chemical or electrostatic interactions with the STM tip, and excitation by tunneling electrons.<sup>5-9</sup>

A basic ingredient to understand the movement of molecules is the evaluation of the molecular adsorption positions, geometries, and potential energy surfaces.<sup>10-14</sup> A particularly important aspect of molecular motion is the understanding of diffusion barriers along the holding surface.

In this work, we study the adsorption of the 4-acetylbiphenyl (ABP) molecule on Au(111). The present calculations are motivated by recent experiments where ABP is shown to be an excellent building block for supramolecular structures that show such a strong individual character that can be manipulated as single objects<sup>7,8,15</sup> at liquid He temperature. In parallel, the weakness of the intermolecular bonding allows ABP to form different structures.<sup>15</sup> The main data<sup>7,8,15</sup> show that more than 90% of the molecules can be moved along the surface  $[1\bar{1}0]$  direction. The rest of the motion involves other directions or a combined motion of rotation and translation. The displacements along the  $[1\bar{1}0]$  direction are 60% in steps of a single lattice unit, and 40% of two lattice units. Very rarely larger steps are found. A defining experimental fact of the different structures is that the molecules adsorb flat on the surface either along the  $[1\bar{1}0]$  direction or the  $[1\bar{1}\bar{2}]$  one. No other possibilities are found. This shows an important directionality and selectivity of the ABP-surface interaction that

is important to unravel for the understanding of supramolecules and overlayers based on biphenyl derivatives.

## Methods

All calculations were performed with the Vienna ab initio simulation package (VASP) using the PBE approximation to density functional theory.<sup>16,17</sup> Valence electrons were described using a plane-wave basis with an energy cutoff of 400 eV and projected-augmented-wave potentials.<sup>18</sup>

We used the Tkatchenko-Scheffler method<sup>19</sup> for the description of the long-range van der Waals (vdW) interactions as implemented in VASP. This method has been shown to reliably describe the adsorption properties of organic molecules on noble-metal surfaces.<sup>20,21</sup> It consists in the use of free-atomic polarizability to compute the coefficient multiplying the  $1/R^6$  behavior, together with a damping function that allows the recovery of the PBE interactions at short range. Here, the Tkatchenko-Scheffler method is applied non-self-consistently such that the dynamical polarization effects are the ones of the PBE functional.

To simulate the surface, we used a Au (111)  $9 \times 5\sqrt{3}$  slab with 4 atomic layers with an inter-slab separation of 20 Å. Structure relaxations were performed until the atomic forces on the molecule and first two layers were smaller than 0.02 eV/Å. The k-point samplings were  $3 \times 3 \times 1$  regular grid of k-points.<sup>22</sup> The coarse PES (here, used for illustrative purposes) were obtained using a smaller unit cell with a  $8 \times 4\sqrt{3}$  slab with 3 atomic layers and one k-point. In order to calculate PES the molecule was systematically placed over the one unit cell with grid sampling  $10 \times 10$  points. In this case the surface and molecule were fixed and single energy point calculations were performed. The total energy was converged below  $10^{-6}$  eV in both cases. The obtained Au bulk lattice constant under the above conditions is 4.114 Å.

We have also used the nudged elastic band method (NEB method)<sup>23</sup> to compute the

minimum-energy path between two conformations on the surface.

The method works by setting an elastic constraint between intermediate conformations and simultaneously allowing them to relax until the minimum energy is attained. The molecule in each position is relaxed but keeps appropriate distance between neighbouring intermediate states (or images). In this way, the obtained energies give the minimum energy path. A critical aspect of the NEB method is the determination of the intermediate states. These images were first calculated by a linear interpolation between initial and final states, and then allowed to relax following the elastic-band constraint. Including the initial and final states, 6 images were sufficient to sample the diffusion pathway.

## Results and Discussion

### The 4-acetylbiphenyl molecule in gas phase

The 4-acetylbiphenyl molecule (ABP) is formed by two isolated phenyl rings and acetyl group. The phenyl rings are joined by a single C-C bond that permits the rings to mutually rotate. The molecule presents an angle between phenyl rings due to the tendency to flatten the molecule in order to optimize the  $\pi$ -conjugation between the rings, and the counterbalancing of steric hindrance between adjacent hydrogens.<sup>24</sup> Our calculations yield an angle of  $35.8^\circ$ . This is  $3.85^\circ$  smaller than the one found for the very similar compound biphenyl-4-carboxaldehyde using quantum chemical methods to reproduce the experimental data.<sup>25</sup> The difference with the present calculation may be caused by the presence of an aldehyde group instead of the acetyl group in our case.

Our calculations confirm the tendency of the phenyl rings to significantly separate from a planar configuration. Figure 1 (A) shows the relaxed molecular structure. The acetyl group replaces the hydrogen atom at the fourth carbon atom in one of the phenyl rings. As a consequence, the molecule develops a small dipole of 1.455 Debyes. The presence of the acetyl group makes possible the formation of hydrogen bonds with similar molecules.

Figure 1 (B) and (C) shows the frontier orbitals of ABP. The highest occupied molecular orbital (HOMO) is a sigma orbital largely concentrated on the acetyl group. It contains an important contribution from the  $2p_x$  orbital of the oxygen atom (taking the  $z$  coordinate as perpendicular to the surface and the  $x$  one along the p-orbital). This feature makes it particularly important to describe the interactions where the O atom is involved. The lowest unoccupied molecular orbital (LUMO) is in contrast a delocalized  $\pi$  orbital extended over the full molecule.

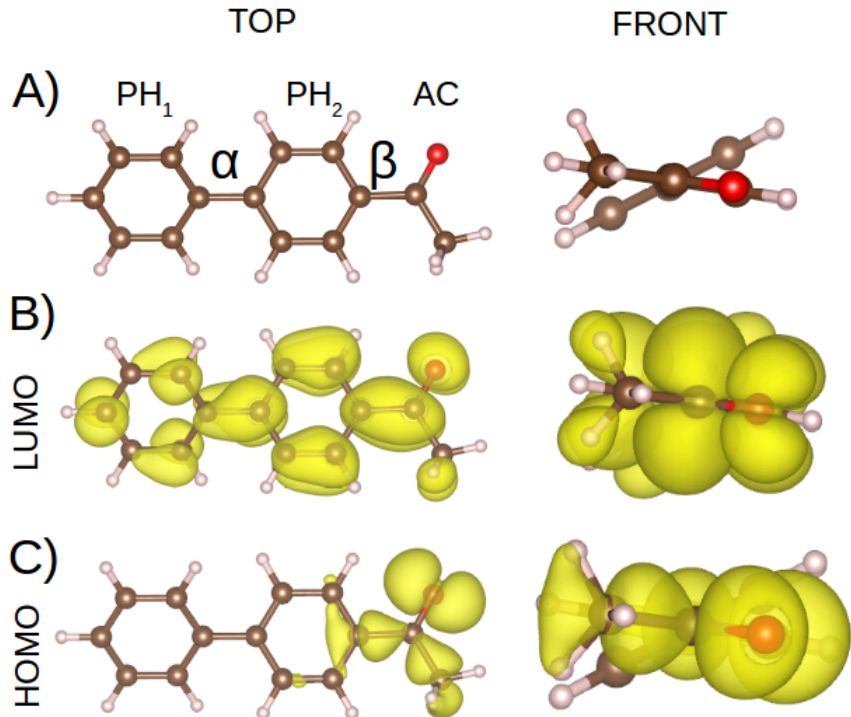


Figure 1: Geometrical structure of ABP molecule A), LUMO B) and HOMO C) orbitals of the ABP molecule.

## The adsorbed molecule

Following the experimental findings of Ref.,<sup>7</sup> we position the molecule in two different conformations. The first one consists in aligning the two phenyl rings with the surface  $[1\bar{1}0]$  direction and the second one with the  $[11\bar{2}]$  direction. The optimization of the two structures entails full relaxation and exploration of the lowest binding energy along the surface unit

cell. As is usually the case for aromatic molecules on Au (111) (see for example Ref.<sup>20</sup>), the phenyl rings optimize their overlap with the surface hollow sites. Figures 2 and 3 show the minimum energy conformations.

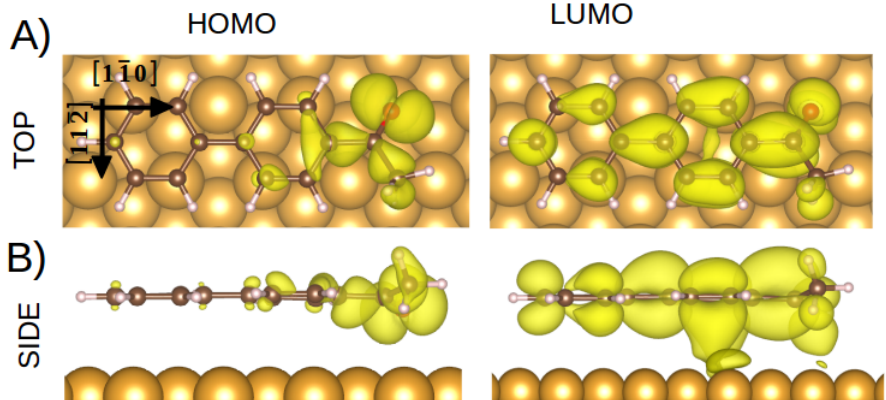


Figure 2: Geometrical structure of ABP molecule adsorbed along the surface  $[1\bar{1}0]$  direction. The yellow contour depicts the shapes of two orbitals of the system that largely match the HOMO and LUMO of the free molecule. The small distortion of the LUMO shows the smallness of covalent-like interactions between molecule and surface. Isosurface of the plot is 0.01.

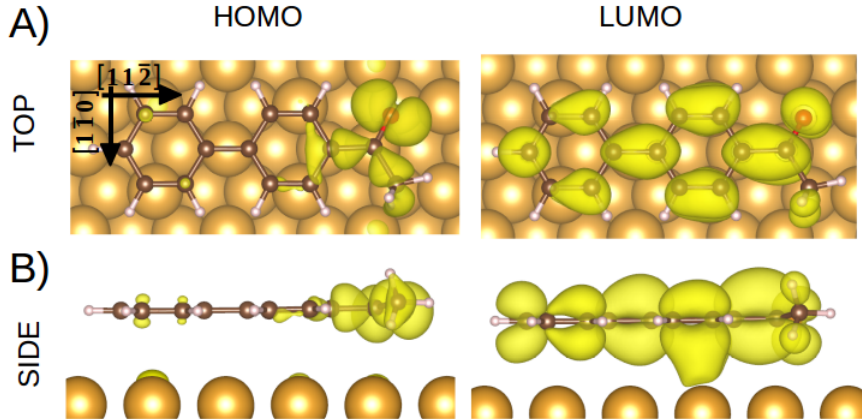


Figure 3: Same as figure 2 for a ABP molecule adsorbed along the surface  $[11\bar{2}]$  direction.

The largest molecular change induced by adsorption is the flattening of the inter-ring angle. The van der Waals interaction is optimized for a large overlap of the ring with the surface, reducing the inter-ring  $\alpha$  angle from  $36^\circ$  to  $3^\circ$  for the  $[1\bar{1}0]$  configuration and  $1^\circ$  for the  $[11\bar{2}]$ , see Table 1. This leads to a stronger conjugation of the  $\pi$ -system induced by the

Table 1: Table of binding energies and geometrical properties of ABP molecule. Distance of  $C_{aver}^n$ -Au[Å] was calculated as a difference of z coordinate averaged over all carbon atoms and z coordinate of first atomic layer.

| Structure           | $E_{ads}$ [eV] | dist. O-Au [Å] | dist. $C_{aver}^n$ -Au[Å] | $\angle \alpha$ [°] | $\angle \beta$ [°] |
|---------------------|----------------|----------------|---------------------------|---------------------|--------------------|
| ABP <sup>free</sup> | —              | —              | —                         | 35.80               | 1.40               |
| ABP <sup>110</sup>  | -1.602         | 2.86           | 3.28                      | 3.10                | 15.20              |
| ABP <sup>112</sup>  | -1.588         | 3.16           | 3.37                      | 0.80                | 6.70               |

adsorption on the surface.

The binding energy, Table 1, is defined by  $E_{ads} = E_{surf+mol} - (E_{surf} + E_{mol})$ . The  $[1\bar{1}0]$  conformation is 14 meV lower than the  $[11\bar{2}]$  one. The binding energy is rather strong around  $-1.6$  eV, very close to the values found for naphtalene and related organic molecules on densely packed noble metal surfaces.<sup>20,21</sup> Moreover, the average height of the molecule to the substrate ( $C_{aver}^n$ -Au, Table 1) is in the same range of distances.<sup>20,21</sup> As in all those cases, the interaction of ABP with Au (111) is given by the vdW interaction between molecule and substrate. Other types of interactions are largely absent.

In addition to the small energy difference between the  $[1\bar{1}0]$  and the  $[11\bar{2}]$  conformations, the acetyl group present different angles (see entry  $\beta$  in Table 1). For the  $[1\bar{1}0]$  conformation the O atom is significantly closer to the surface leading to an acetyl angle twice as large. These two differences are connected and show the interaction of the O atom with one of the top Au atoms of the surface. Two states reminiscent of the LUMO and HOMO are plotted in figures 2 and 3. They show very small differences compared to the molecule in the gas phase (Fig. 1) due to the very weak O-Au interaction.

Charge transfer between molecule and surface is also absent. Bader analysis<sup>26</sup> leads to less than 0.1 electrons of reduction of the molecular electrons. As a consequence, all interatomic distances within the molecule are identical to the gas phase ones within numerical accuracy. Despite the absence of charge transfer, there is a polarization of the electronic clouds locally around molecule and substrate, that point at the importance of vdW interactions in this system, figure 4. The induced density is defined as the difference of electronic density between the adsorbed system and the sum of the surface and molecular densities keeping

the same geometry but separately computed. As expected, the differences between both conformations reduces to the difference in oxygen position with respect to the surface.

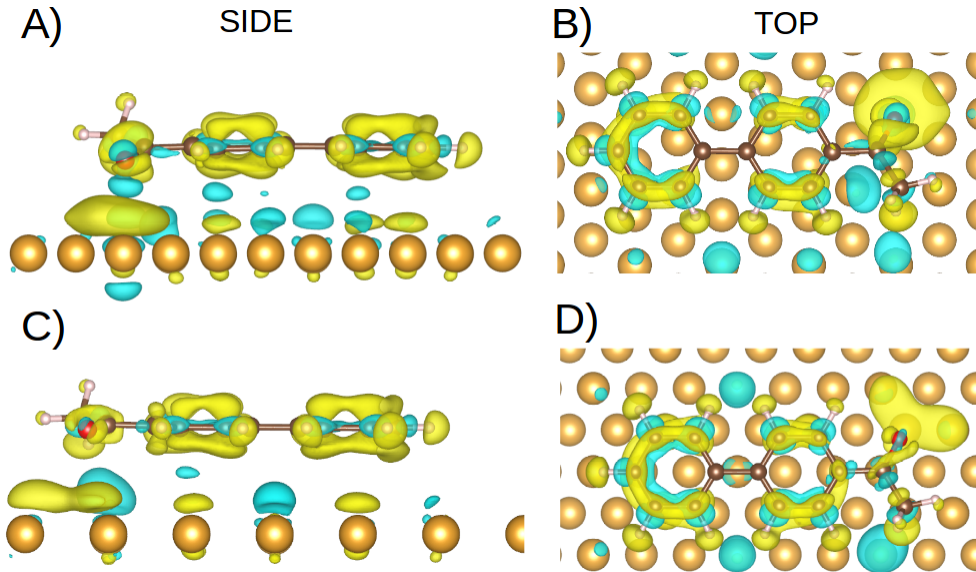


Figure 4: Induced density of ABP in  $[1\bar{1}0]$  A),B) and ABP in  $[11\bar{2}]$  C),D). The main difference involves the induced density about the oxygen atom and the area underneath the oxygen atom. The isosurface of the plot is  $0.0005 \text{ e}/\text{\AA}^3$  and yellow and green colors denote positive and negative values respectively.

The small overlap of the LUMO with surface states in figures 2 and 3 does explain the 0.5 eV downward shifting and broadening of the LUMO in the projected density of states (PDOS), see figure 5. The blue line corresponds to the PDOS of the gas-phase molecule, while the red and green refer to the PDOS of the  $[1\bar{1}0]$  and  $[11\bar{2}]$  conformations. As gleaned from figures 2 and 3 the overlaps between the LUMOs of both configurations and the substrate are the same leading to equal PDOS. However, the behavior of the HOMO is more intricate.

The molecular orbital structures on the surface are determined by the molecule-surface interactions and referred to the surface Fermi energy dividing between occupied and empty electronic states. The gas-phase molecular structure is aligned to the ones on the surface using their respective vacuum levels. The HOMO contribution is the first occupied peak, just below the Fermi level (the zero of energies in figure 5). We see that the gas-phase HOMO coincides with the HOMO for the  $[11\bar{2}]$  conformation, and that the HOMO – HOMO-1



distance is maintained. However, the  $[1\bar{1}0]$  conformation shows a downward shift of 0.5 eV and a closing of the HOMO – HOMO-1 distance. We rationalize these shifts by the larger interaction of the O atom with the surface for the  $[1\bar{1}0]$  case as described above. Indeed, the important contribution of the O  $p$ -orbital to the HOMO, makes it shift due to the interactions caused by the O atom. These interactions are smaller or even absent in the other orbitals where the relative weight of the O atom is lesser. Nevertheless, the bonding analysis is better performed in terms of the electronic density and its derivatives instead of the molecular orbitals. A clear example of this is given by the NCIPLOT methodology applied to molecules,<sup>27</sup> periodic systems<sup>28</sup> and the organic-metal surface interface.<sup>29</sup>

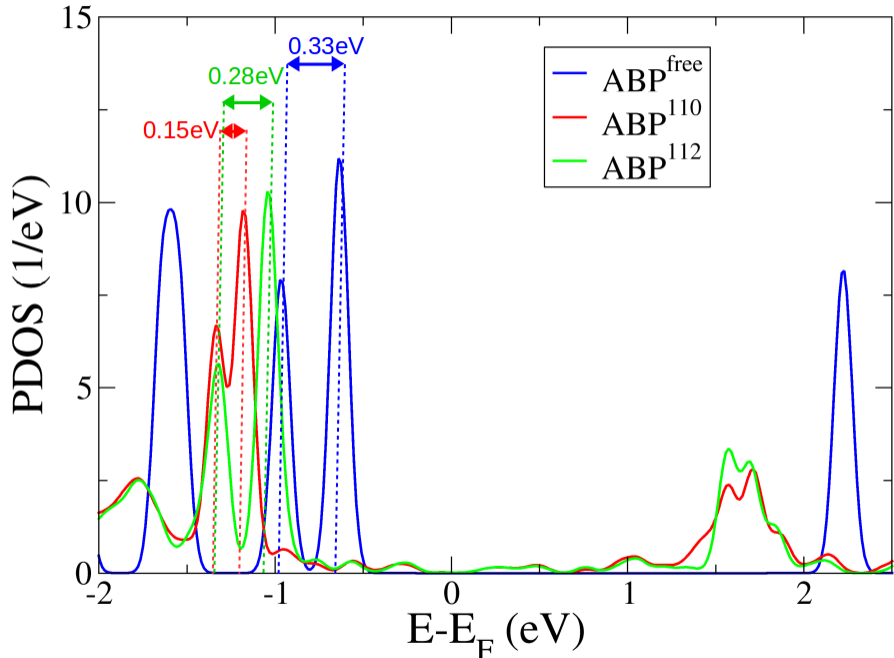


Figure 5: Density of states projected on the orbitals of the ABP molecule in the gas phase (marked as “free” and plotted in blue color) and the adsorbed molecule along the  $[1\bar{1}0]$  direction (red color) and along the  $[11\bar{2}]$  one (green color). The vacuum level of the surface and gas-phase systems have been aligned. This shows a sizable downshift in energies with modification of the density of states due to the interaction between molecule and substrate.

## Diffusion barriers along the Au (111) surface

Ample experimental results<sup>7</sup> show that ABP diffuses on the Au (111) surface. The experiments report on the formation of supramolecular structures<sup>7</sup> that themselves can be controllably moved by applying electronic pulses from an STM. Study of these manipulations show that the ABP molecules preferentially move along the high-symmetry directions of the surface and in small integer steps of the surface lattice parameter. These findings are unexpected for a vdW-bonded molecule, because the vdW interaction shows a very small corrugation with surface sites. Rather, a uniform potential energy surface (PES) is expected with barriers that are negligible compared to the overall binding energy. It is interesting then to compute and rationalize the barriers that ABP encounters when diffusing along the surface.

Figure 6 shows the adiabatic PES along four directions. The first two (red and blue) are for a molecule adsorbed along the  $[1\bar{1}0]$  direction. The red curve is a path following the  $[1\bar{1}0]$  direction when  $0^\circ$  is between molecule axis and path as marked on the figure 2. We see that 5 images suffice to yield a smooth representation of the PES. The barrier is less than 40 meV. Compared to the 1.6 eV of binding energy of the ABP molecule with  $[1\bar{1}0]$  orientation, we can conclude that the barrier is indeed small. The blue path presents a stronger barrier of roughly 80 meV. Again, this is a small corrugation of the PES.

The blue path is for a molecule moving along a  $[1\bar{1}0]$  direction rotated  $60^\circ$  with respect to the original  $[1\bar{1}0]$  direction. The barrier is much higher because the molecule is not aligned with the moving direction. Table 2 gives the barrier values and the contribution of vdW interactions to the barrier ( $E^{disp}_{barrier}$ ). We can see that the vdW interaction alone accounts for the barrier. The 80-meV barrier is then the corrugation of vdW landscape of the ABP molecule on Au (111).

When the molecule is adsorbed along the  $[11\bar{2}]$  direction, figure 3, the barriers also depend on what  $[11\bar{2}]$  direction is taken with respect to the molecule, figure 6, cyan and green curves. The vdW corrugation suffices to explain the barriers. Only when the barriers are small, do

other corrugations play a role. Indeed, the small changes in conformation of the molecule as it is pushed above the barrier explain the contributions to the barrier that are not 100% vdW.

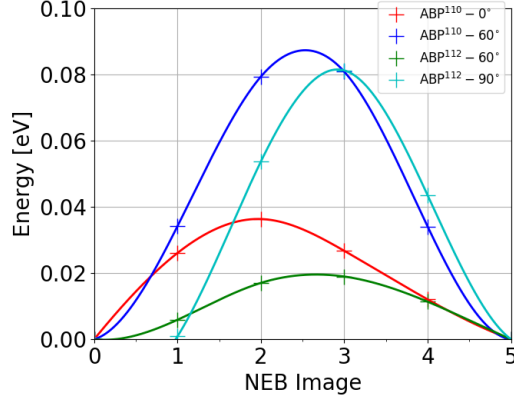


Figure 6: Chosen directions along the adiabatic potential energy surface calculated by NEB for a molecule adsorbed along the  $[1\bar{1}0]$  direction ( $ABP^{1\bar{1}0}$ ) and along the  $[11\bar{2}]$  direction ( $ABP^{11\bar{2}}$ ). For the  $ABP^{1\bar{1}0}$  case the molecule is moved in one of the 3 equivalent  $[1\bar{1}0]$  directions of the Au (111) surface. For the  $0^\circ$  case the molecule follows the same direction it points at (red line). For the  $60^\circ$  one, the molecule follows a  $[1\bar{1}0]$  direction that makes a  $60^\circ$  angle with the direction of the molecule (blue line). The  $ABP^{11\bar{2}}$  molecule along a  $60^\circ$  path finds a very small barrier (green line). However, the  $ABP^{11\bar{2}}$  molecule finds the maximum barrier when it is moved along a  $[1\bar{1}0]$  direction, the  $90^\circ$  case (cyan line). Energy points of the barriers were fitted by cubic spline.

Table 2: Table of energy barriers.

| Structure/direction        | $E_{barrier}^{tot}$ [eV] | $E_{barrier}^{disp}$ [eV] |
|----------------------------|--------------------------|---------------------------|
| $ABP^{1\bar{1}0}-0^\circ$  | 0.036                    | 0.023                     |
| $ABP^{1\bar{1}0}-60^\circ$ | 0.087                    | 0.080                     |
| $ABP^{11\bar{2}}-60^\circ$ | 0.019                    | 0.009                     |
| $ABP^{11\bar{2}}-90^\circ$ | 0.081                    | 0.070                     |

A clearer representation of the above paths, figure 6, can be seen in figure 7 where the center of mass of the molecule has been displaced along the surface and the internal coordinates have been maintained in the minimum energy configuration. This approximate representation is intended for visualization purposes. Now, the directions given in figure 6 can be easily pictured. The PES profiles allow us to conclude that there is one preferred direction of diffusion for each configuration, as well as a less preferred direction. These observations

may play a role in the explanation of the collective uniform diffusion of supramolecular structures composed of ABP molecules.

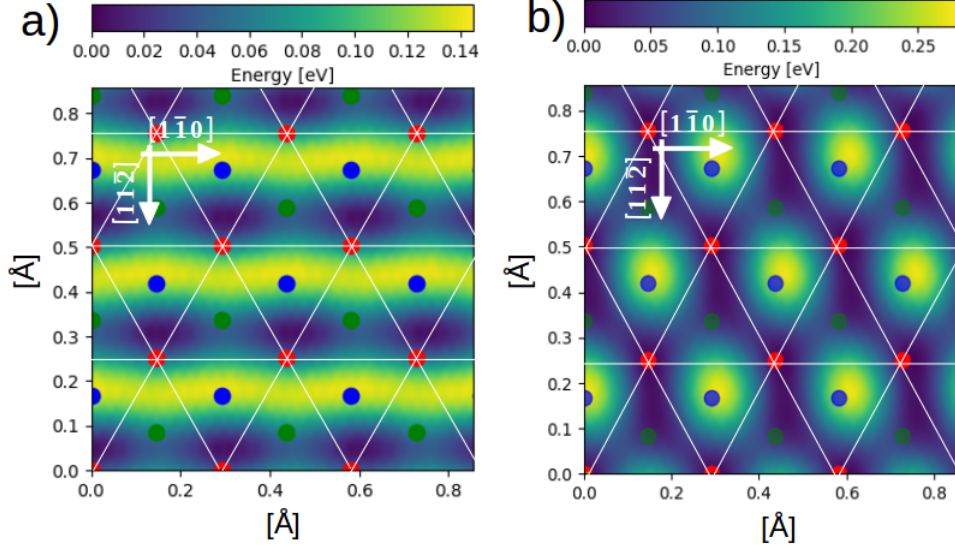


Figure 7: Potential energy surfaces of ABP with its axis along the  $[1\bar{1}0]$  direction a) and  $[11\bar{2}]$  direction b) Red, blue, green dots indicate position of Au atoms in first, second and third layer. White straight lines are an eye-guide for Au rows in first layer. In agreement with the NEB paths of figure 6, we see that the barrier is minimum along the  $[1\bar{1}0]$  direction that aligns with the molecular axis.

A contribution to the barrier and, hence, to the directionality of the interactions is given by the distortion of the molecule. In order to estimate the distortion, we have compared the nuclear positions of the molecular atoms along the NEB path. In figure 8 we compute

$$\text{delta} = \sum_{\text{atom}} |\vec{R}_{NEB} - \vec{R}_{relaxed}| \quad (1)$$

where  $\vec{R}_{NEB}$  are the coordinates of each atom for a given NEB image and  $\vec{R}_{relaxed}$  are the coordinates for the relaxed molecules, where the center of mass has been shifted to agree in the compared configurations. At the moment of the transition, we find an accumulated displacement of 1 Å in the coordinates of the molecule, which amounts to an average displacement of more than 0.05 Å per carbon atom. This goes in the direction of the increase of energy as we move through the transition state.

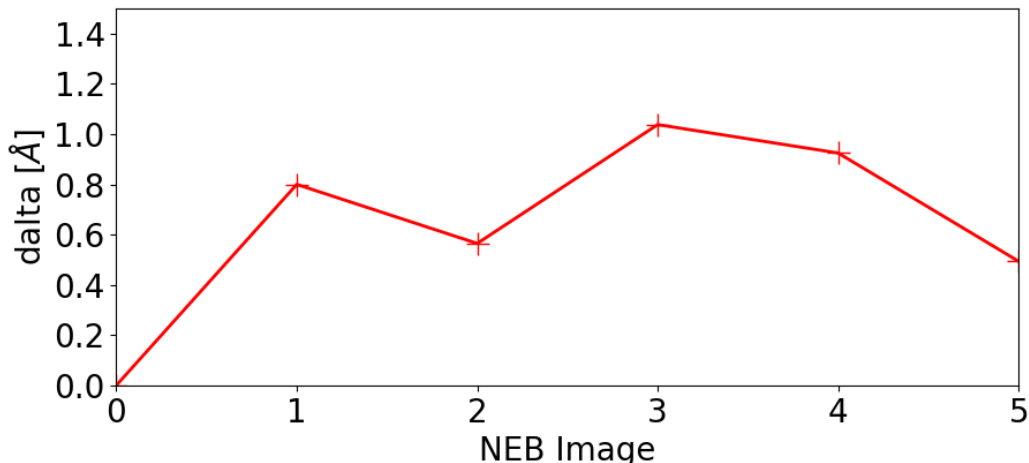


Figure 8: Accumulated displacement of the molecular atomic positions once the center of mass has been shifted together. Molecule is moved in the  $[11\bar{2}]$  direction. The geometrical distortion is maximum at the transition state, in agreement with a geometrical interpretation of the diffusion barrier.

An important contribution for the vdW interaction comes from the polarization of the different components of the system. The induced electronic density permits us to assess the change of the polarization as the molecule moves through its diffusion path given by the NEB calculation. Figure 9 shows the change of induced density for the different images of the NEB calculation. We see that the phenyl rings are little affected by polarization while the oxygen atom suffers important perturbation as it moves over the surface, particularly images 1 and 2. The polarization is very local and it is mainly due to the Au–O interaction. The oxygen atom is largely inert at the molecule but it is easily polarizable as the polarization included in the PBE functional shows.

These results show that simpler molecular dynamics methods with simple potentials will fail to capture the large polarizability of the metallic surface, where the PBE functional is adequate.

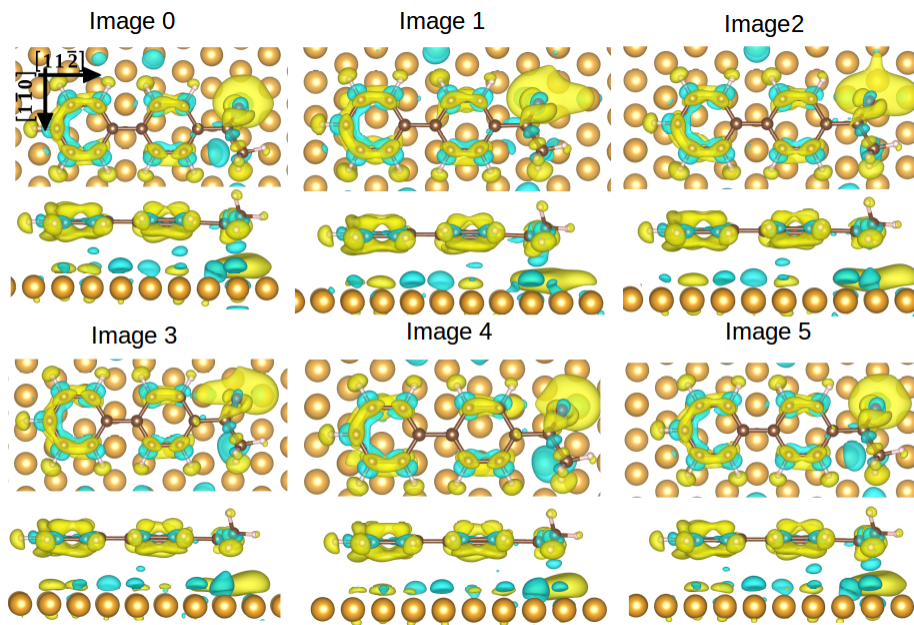


Figure 9: Induced electronic density as the molecule conformation changes along the different images of the minimum-energy path given by the NEB calculation. The molecule is translated in  $[11\bar{2}]$  direction. Largely the oxygen atom is polarized as it changes its registry with the surface. The polarization of this calculation is the one given by the PBE functional.

## Conclusions

This study reveals the adsorption properties of 4-acetylbiphenyl on Au (111) that are important to rationalize the atomic manipulations performed with an STM in Ref.<sup>7</sup> As with other aromatic molecules adsorbed on noble metal surfaces, van der Waals interactions are the prevailing interactions. As a consequence, very small molecular changes happen during adsorption, except for the flattening of the two phenyl rings. Due to the small perturbation exerted by the surface on the molecule, charge transfer is less than 0.1 electrons and molecular orbitals are easily recognized on the adsorbed molecule.

The main experimental data<sup>7,8,15</sup> are that the molecules adsorb flat on the surface either along the  $[11\bar{0}]$  direction or the  $[11\bar{2}]$  one and that they diffuse (more than 90%) along the  $[11\bar{0}]$  direction in steps of one or two surface-lattice parameter. These data can be rationalized by the corrugation of the vdW interaction. Indeed, the vdW interaction follows the corrugation of the surface, as a consequence the molecule will follow steps matching units

of the surface-lattice parameter. The fact that only one or two steps are experimentally available means that a sizeable damping of the motion is available probably given to the continuum of electronic excitations available from zero energy on a metallic surface.

Unfortunately, no experimental barrier has been obtained. The computed PES show adiabatic barriers are below 90 meV. Experimentally, the molecule is moved when bias pulses larger than 2 volts are applied. This means that electrons from the STM tip need to reach 2 eV before some molecular dynamics can be detected. However, this is not connected with the molecular energy barriers but rather with the energy-dependence of the electron-molecule cross section. Our density of state shows that the molecular states lie at biases in the eV range facilitating the electron-molecular collision at eV energies.

The computed barriers are negligible in front of the binding energy of the surface (-1.6 eV). This corroborates the common idea that van der Waals interactions lead to rather flat PES. Our calculations further show that the intrinsic dipole of the molecule is too small to play a role in the adsorption or diffusion of the molecule.

This work has permitted us to rationalize in terms of the van der Waals interaction that at a few K of temperature, the molecules stably adsorb, can assemble and be easily manipulated with a scanning probe, as experimentally found.<sup>7</sup>

## Acknowledgement

We acknowledge the EU commission H2020 FETopen program *Mechanics with Molecules*, project number 766864. We are also grateful for financial support from the Spanish MICINN, project RTI2018-097895-B-C44. Computer resources were obtained at the RES computers Finisterrae II in project RES-QCM-2019-1-0024 and Cibeles in project RES-QS-2019-3-0012 and are gratefully acknowledged.

## References

- (1) Clair, S.; De Oteyza, D. G. Controlling a Chemical Coupling Reaction on a Surface: Tools and Strategies for On-Surface Synthesis. *Chemical Reviews* **2019**, *119*, 4717–4776.
- (2) Tsutsui, M.; Taniguchi, M. Single molecule electronics and devices. *Sensors (Basel, Switzerland)* **2012**, *12*, 7259–98.
- (3) Bottari, G.; de la Torre, G.; Guldi, D. M.; Torres, T. Covalent and Noncovalent Phthalocyanine-Carbon Nanostructure Systems Synthesis, Photoinduced Electron Transfer. *Chem Rev* **2010**, 6768–6816.
- (4) Rosei, F.; Schunack, M.; Naitoh, Y.; Jiang, P.; Gourdon, A.; Laegsgaard, E.; Stensgaard, I.; Joachim, C.; Besenbacher, F. *Progress in Surface Science*; 2003; Vol. 71; pp 95–146.
- (5) Morgenstern, K.; Lorente, N.; Rieder, K.-H. *Physica Status Solidi (B)*; 2013; Vol. 250; pp 1671–1751.
- (6) Eisenhut, F.; Meyer, J.; Krüger, J.; Ohmann, R.; Cuniberti, G.; Moresco, F. Inducing the controlled rotation of single o-MeO-DMBI molecules anchored on Au(111). *Surface Science* **2018**, 0–1.
- (7) Nickel, A.; Ohmann, R.; Meyer, J.; Grisolia, M.; Joachim, C.; Moresco, F.; Cuniberti, G. Moving nanostructures: Pulse-induced positioning of supramolecular assemblies. *ACS Nano* **2013**, *7*, 191–197.
- (8) Ohmann, R.; Meyer, J.; Nickel, A.; Echeverria, J.; Grisolia, M.; Joachim, C.; Moresco, F.; Cuniberti, G. Supramolecular Rotor and Translator at Work: On-Surface Movement of Single Atoms. *ACS Nano* **2015**, *9*, 8394–8400.
- (9) Simpson, G. J.; García-López, V.; Petermeier, P.; Grill, L.; Tour, J. M. How to build and race a fast nanocar. *Nature Nanotechnology* **2017**, *12*, 604–606.



- (10) Zhang, H.; Chi, L. GoldOrganic Hybrids: On-Surface Synthesis and Perspectives. *Advanced Materials* **2016**, *28*, 10492–10498.
- (11) Liu, W.; Carrasco, J.; Santra, B.; Michaelides, A.; Scheffler, M.; Tkatchenko, A. Benzene adsorbed on metals: Concerted effect of covalency and van der Waals bonding. *Physical Review B - Condensed Matter and Materials Physics* **2012**, *86*, 1–6.
- (12) Peköz, R.; Donadio, D. Effect of van der Waals interactions on the chemisorption and physisorption of phenol and phenoxy on metal surfaces. *Journal of Chemical Physics* **2016**, *145*.
- (13) Martínez, J. I.; Abad, E.; González, C.; Ortega, J.; Flores, F. Theoretical characterization of the TTF/Au (1 1 1) interface: STM imaging, band alignment and charging energy. *Organic Electronics: physics, materials, applications* **2012**, *13*, 399–408.
- (14) Meyer, R.; Lemire, C.; Shaikhutdinov, S. K.; Freund, H. J. Surface chemistry of catalysis by gold. *Gold Bulletin* **2004**, *37*, 72–124.
- (15) Eisenhut, Frank;; Durand, Corentin;; Moresco, Francesca;; Launay, Jean-Pierre;; Joachim, Christian, Training for the 1st international nano-car race: the Dresden molecule-vehicle. *Eur. Phys. J. Appl. Phys.* **2016**, *76*, 10001.
- (16) Kresse, G.; Furthmüller, J. Efficiency of ab-initio total energy calculations for metals and semiconductors using a plane-wave basis set. *Computational Materials Science* **1996**, *6*, 15 – 50.
- (17) Perdew, J. P.; Burke, K.; Ernzerhof, M. Generalized Gradient Approximation Made Simple. *Physical Review Letters* **1996**, *77*, 3865.
- (18) Kresse, G.; Joubert, D. From ultrasoft pseudopotentials to the projector augmented-wave method. *Phys. Rev. B* **1999**, *59*, 1758–1775.

- (19) Tkatchenko, A.; Scheffler, M. Accurate Molecular Van Der Waals Interactions from Ground-State Electron Density and Free-Atom Reference Data. *Phys. Rev. Lett.* **2009**, *102*, 073005.
- (20) Maurer, R. J.; Ruiz, V. G.; Camarillo-Cisneros, J.; Liu, W.; Ferri, N.; Reuter, K.; Tkatchenko, A. Adsorption structures and energetics of molecules on metal surfaces: Bridging experiment and theory. *Progress in Surface Science* **2016**, *91*, 72 – 100.
- (21) Scarbath-Evers, L. K.; Todorović, M.; Golze, D.; Hammer, R.; Widdra, W.; Sebastiani, D.; Rinke, P. Gold diggers: Altered reconstruction of the gold surface by physisorbed aromatic oligomers. *Phys. Rev. Materials* **2019**, *3*, 011601.
- (22) Monkhorst, H. J.; Pack, J. D. Special points for Brillouin-zone integrations. *Phys. Rev. B* **1976**, *13*, 5188–5192.
- (23) Jónsson, H.; Mills, G.; Jacobsen, K. In *Classical and Quantum Dynamics in Condensed Phase Simulations*; Berne, B., Ciccotti, G., Jacobsen, K., Eds.; World Scientific: Singapore, 1998; p 385.
- (24) Johansson, M. P.; Olsen, J. Torsional Barriers and Equilibrium Angle of Biphenyl: Reconciling Theory with Experiment. *Journal of Chemical Theory and Computation* **2008**, *4*, 1460–1471, PMID: 26621432.
- (25) Srishailam, K.; Reddy, B. V.; Rao, G. R. Investigation of torsional potentials, hindered rotation, molecular structure and vibrational properties of some biphenyl carboxaldehydes using spectroscopic techniques and density functional formalism. *Journal of Molecular Structure* **2019**, *1196*, 139 – 161.
- (26) Henkelman, G.; Arnaldsson, A.; Jónsson, H. A fast and robust algorithm for Bader decomposition of charge density. *Computational Materials Science* **2006**, *36*, 354–360.

- (27) Johnson, E. R.; Keinan, S.; Mori-Sánchez, P.; Contreras-García, J.; Cohen, A. J.; Yang, W. Revealing Noncovalent Interactions. *Journal of the American Chemical Society* **2010**, *132*, 6498–6506.
- (28) Otero-de-la Roza, A.; Johnson, E. R.; Contreras-García, J. Revealing non-covalent interactions in solids: NCI plots revisited. *Physical Chemistry Chemical Physics* **2012**, *14*, 12165–12172.
- (29) Boto, R. A.; Contreras-García, J.; Calatayud, M. The role of dispersion forces in metal-supported self-assembled monolayers. *Computational and Theoretical Chemistry* **2015**, *1053*, 322–327.

## Graphical TOC Entry

